J. Non-Equilib. Thermodyn.
Vol. 22 (1997), pages 1–19

Review Article

Bénard Convection Flows

J. Bragard, M. G. Velarde
Instituto Pluridisciplinar, Universidad Complutense de Madrid, Madrid, Spain

Registration Number 745

Abstract

A review is provided of salient findings, old and recent, about Bénard convection flows in a liquid layer heated from below and open to the ambient air. Instability and subsequent convective patterns past the instability threshold are the consequence of surface tension gradients acting along the open surface and by the temperature gradient maintained across the liquid layer. The onset of hexagons, rolls, squares and their relative stability is described here as well as the appearance of more complex patterns like labyrinthine convection flows. Asymptotic unsteadiness is also expected near the instability threshold as a consequence of the non-variational character of the problem, hence a precursor of space-time chaos, interfacial turbulence already possible at low Marangoni number.

1. Introduction

In the vicinity of the surface of separation between two different fluids, the thermodynamic properties (such as density, composition, viscosities,...) undergo strong variations on a very small scale (the interfacial phase thickness is of the order of molecular size) [1]. In equilibrium configurations these rapid variations can be characterised by an energy per unit area, that is commonly referred to interfacial tension (for liquid/gas interfaces, it is usually called surface tension). Then to a first approximation, this allows to consider the interface as a mere surface of discontinuity in the above mentioned variables. The interfacial tension σ usually depends on the scalar fields in the system (e.g. the electrical field, the temperature field), as well as on the concentration of foreign materials on the interface, generally called surfactants [2] . Interfacial gradients leading to tangential stresses may generate motions at the interface, that, due to continuity and viscosity, extend in the bulk of the adjacent liquids. This phenomenon, called Marangoni effect leads to either thermocapillary convection (driving gradient is of thermal origin) or solutocapillary convection (due to composition gradients). Convection may appear as stationary motion, oscillations (waves), or interfacial turbulence. In this paper, we shall deal with the Bénard-

Marangoni convection that occurs when the gradient is perpendicular to the interface and oriented downwards to a liquid layer open to air.

When a thin fluid layer is heated from below the motionless state is unstable if the vertical temperature gradient overcomes a threshold value imposed by viscosity and heat diffusivity that tend to stop or slow down motion and homogenize the temperature distribution, respectively. The surface tension gradient-driven transition from the motionless conduction state to a convective state in which the fluid motion exhibits a patterned structure (convective cells: hexagons, squares or rolls) was first systematically studied by Bénard [3] though he did not clarify enough the relevant role played by the surface tension (see [4–6]). The rationale for the instability goes as follows. We assume a spontaneous temperature disturbance at the open surface; e.g. a cooling (marked- in Fig. 1). Therefore, at this point, the surface tension is higher (in general, the surface tension is a decreasing function of temperature), and the surface tends to shrink, dragging by viscosity the fluid toward this cold point. By conservation of mass, the fluid sinks in the bulk and rises at the surface away from the cold spot. The initial perturbation will originate a convective motion if the rising hot fluid (marked $+$) has a sufficient high temperature in order to maintain the surface temperature gradient, i.e. if the temperature difference between the top and bottom of the layer (ΔT) reaches a critical value. The factors tending to prevent the convection are heat diffusion and viscosity. Then we have a destabilising mechanism injecting energy into the system through the surface tension gradient: $-(\partial\sigma/\partial T)\Delta T$ and friction with dissipation: viscosity (μ) and heat (κ). The energy or force balance between these two oposing processes can be best expressed with a dimensionless parameter, the Marangoni number: $Ma = \dfrac{-(\partial\sigma/\partial T)\Delta T h}{\mu\kappa}$. This quantity can also be considered as a Reynolds number or, more appropriately, as a Péclet number.

In the following sections, we study the transition between the two states, conduction to convection. First, we write the governing equations of the system for mass, momentum and energy, and the boundary conditions. Generally, these equations are difficult to solve in compact analytical form, so we shall use numerical methods and/or we shall simplify the original equations down to a tractable, albeit relevant problem. A method is to linearize the equations and boundary conditions, then solve them to find the linearized solution. Linear theory and the corresponding linear stability analysis yield sufficient conditions for instability. Then building on linear results we may try further

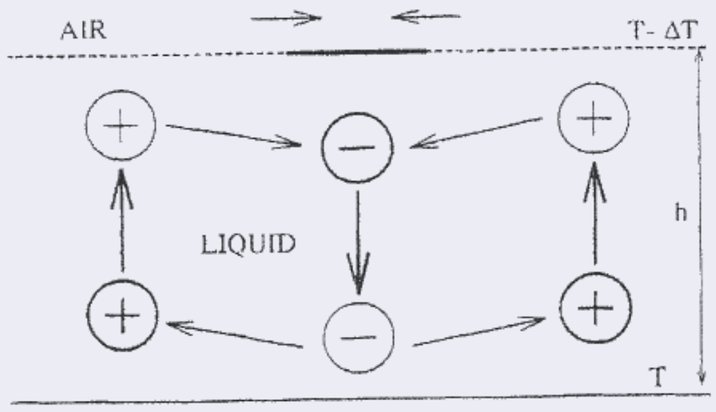

Fig. 1: Sketch of the Bénard-Marangoni instability.

progress into the original nonlinear problem by using perturbative methods (asymptotic, multiple-scales methods). Perturbative methods allow getting approximations to the nonlinear solution (e.g. higher order corrections to the velocity profile), removing degeneracies due to the linearization and assessing the stability of the (linear) solutions.

The paper is organised as follows. Section 2 contains an historical introduction. In Section 3 we recall the amplitude equations for supercritical, cellular flows. In Section 4 we present the results of the integration of these equations. Section 5 deals with the Eckhaus instability. In Section 6 we discuss the evolution of defects and the appearance of complex convective structures. In Section 7 we provide some conclusions.

2. Remarks of historical interest

The systematic experimental research on patterned convection began with H. Bénard [3] although earlier authors reported phenomena similar to the findings of Bénard [7–9] (see also [10]). Bénard set an example for virtually all subsequent experiments on convection in shallow horizontal fluid layers by supplying uniform heating from below and trying to eliminate the influence of the lateral confinement of the fluid. The major finding of Bénard was the discovery of hexagonal convection cells which are now commonly referred to as Bénard cells [5, 6]. The circulation of the fluid in the hexagonal cells is generally upwards in the center (up-hexagons) and downwards along the rim. Optical studies also showed that the surface of the fluid is depressed over the center of the cells. The deformation of the surface is about a micron for a spermaceti layer about one millimeter deep and $\Delta T \sim 80\,\mathrm{K}$. Bénard also found that the ratio of the distance between the cell centers and the depth of the fluid is constant, at least to a first approximation, hence defining a universal dimensionless wavelength at threshold.

Although Bénard was aware of the role of surface tension and surface tension gradients in his experiments, it took, however, five decades to unambiguously assess, experimentally and theoretically, that indeed the surface tension gradient rather than buoyancy was the cause of Bénard cells in thin liquid films [4, 11–13]. The first author to explain the effect of the surface tension gradients on Bénard convection was Pearson [14]. According to Pearson's theory, for a critical Marangoni number Ma_c the layer displays a specific short wave pattern of stationary cellular convection. The actual value of Ma_c depends on boundary conditions, e.g. for a liquid layer resting on a heated copper plate and open to air $Ma_c \approx 80$ and $k_c \approx 2$.

Since these pioneering works many publications have been devoted to the Marangoni instability of a Bénard layer, in both experimental and theoretical directions. The review articles by Normand, Pomeau and Velarde [4] and by Davis [15] discuss the role of both buoyancy and surface tension gradients in triggering convective instability. Recently, a review article by Cross and Hohenberg [16] was devoted to non-equilibrium pattern formation, with a sketchy section dealing with genuine Bénard cells i.e. Bénard-Marangoni convection. Koschmieder who has been for decades a key figure in the experimental investigation of the Bénard problem wrote recently a very valuable monograph [6]. There are still challenging problems like relative stability of patterns, higher transitions and interfacial turbulence, a case of space-time chaos with

high dissipation (high Peclet number flows at variance with mostly inertial high Reynolds number turbulent flows).

To cope with the analytical difficulties of Navier-Stokes and Fourier equations, one has the alternative of numerical integration, albeit in limiting cases (like with fluids having large Prandtl number) as done e.g. by Thess and Orzag [17], or to develop a weakly non-linear approach around instability thresholds as Landau did for phase transitions. Perturbative methods were first applied to steady Bénard-Marangoni convection by Scanlon and Segel [18] who used very drastic, albeit relevant simplifications, i.e. infinite Prandtl number and semi-infinite fluid layer. This same approximation was latter used by Levchenko and Chernyakov [19] and by Velarde and collaborators [20–22] to discuss interfacial waves in Bénard layers. Scanlon and Segel predicted the selection of an hexagonal convective pattern in favor of rolls above the onset of instability. They also showed that the hexagonal structure may be stable for subcritical values of the Marangoni number. The theory of Scanlon and Segel was significantly improved by Cloot and Lebon [23] and by Bragard and Lebon [24].

Experimental investigations increased our knowledge of the problem. For instance, following earlier work by Koschmieder, Cerisier *et al.* [25] studied the relative stability of rolls and hexagons, and concluded that hexagons are less stable relative to rolls when the depth of the fluid is increased. This result is in good ageement with the result obtained by Lebon and collaborators [23, 24] who predicted a transition from hexagons to rolls for high Marangoni numbers. They also predicted the existence of a range where both hexagons and roll patterns can coexist. A recent experiment [26] has shown the hysteretic behavior occurring in Bénard-Marangoni convection. This is to be expected in view of the discrepancy existing between energy and linear stability approaches to the problem [27–29]. The hysteresis appears in a 3% subcritical range where both conduction and convective hexagonal motion can coexist. Schatz *et al.* found a critical Marangoni number of 84 very close to the predicted value by Pearson (i.e. $Ma_c = 79.6$). Another recent experiment [30] shows a secondary instability from a perfectly hexagonal pattern to a square pattern. The experimental set-up used by the latter authors differs from that used by Bénard because the gas layer at the upper surface is very thin and consequently in a rather drastic way affects the thermal boundary condition at the interface between the fluid and gas layer, a point earlier remarked by Koschmieder [6]. Recently, we have derived the amplitude equation for the modes of convection above threshold, taking care of the dependence of the coefficients of these equations on various dimensionless parameters of the system, including various thermal boundary conditions, through a varying, suitable Biot number (to be defined below) [31]. Our amplitude equations together with the appropriate boundary conditions for Bénard-Marangoni convection yield various possible solutions. These include convective patterns like hexagons, rolls, and squares, a transition from an hexagonal structure to a labyrinthine structure when the size of the system is large enough (lateral size of the container of the order of one hundred wavelengths), and unsteadiness, like a precursor of interfacial turbulence. Several other authors have taken an approach similar to ours to explore various issues [32–36].

3. Evolution toward patterned convection

Close to the instability threshold the system may be described by amplitude equations having a universal form [4, 16, 18, 37–39]. The coefficients of these amplitude equations are specific to each instability, they depend on the dimensionless numbers of the problem, hence fluid properties, boundary conditions, and on the external forcing. In our problem, disregarding aspect ratio (relative lateral size to liquid depth) three dimensionless numbers are relevant:

$$Pr = \frac{\nu}{\kappa};\ Ma = -\frac{\partial\sigma}{\partial T}\frac{d\Delta T}{\kappa\eta};\ Bi = \frac{hd}{k} \tag{1}$$

which are the Prandtl, Marangoni and Biot numbers, respectively. The quantities ν and κ are the kinematic and thermal diffusivity, respectively, σ is the surface tension, d is the thickness of the layer, ΔT is the temperature difference between the open surface and the bottom plate taken positive when the heating is from the liquid size. η is the dynamic viscosity, h is the thermal surface conductance and k is the thermal conductivity of the fluid layer. The Prandtl number is an intrinsic property of the fluid. The Biot number defines the heat transfer at boundaries: a large (infinite) value of the Biot number corresponds to a perfectly conducting boundary, and a vanishing value corresponds to a poorly conducting surface.

We start with the standard incompressible fluid mechanics equations: Navier-Stokes, continuity and energy equations, that we take in the Boussinesq approximation [40–44]. The assumption of an undeformed open surface corresponds to the limit of strong surface tension. The validity of this assumption is a subtle question [15, 29] but for a vanishing capillary number, except in the long wave limit $k \to 0$, we can assume with no loss of generality a flat interface. In the case of a one millimeter deep silicone oil, the capillary number takes the value:

$$Ca = \frac{\mu\kappa}{\sigma_0 d} = 5.6 \cdot 10^{-4}.$$

Using appropriate scales for time, space, velocity, pressure and so on the problem is then in dimensionless form:

$$\frac{\partial \mathbf{v}}{\partial t} + (\mathbf{v}\cdot\nabla)\mathbf{v} = Pr(-\nabla p + \Delta\mathbf{v})$$

$$\nabla\cdot\mathbf{v} = 0 \tag{2}$$

$$\frac{\partial T}{\partial t} + \mathbf{v}\cdot\nabla T = \Delta T.$$

Note that for simplicity and as we shall consider no surface deformation and quite thin layers like in most of Bénard experiments we disregard gravity. The boundary

conditions are: at the lower uniformly heated rigid plate:

$$\mathbf{v} = 0 \tag{3}$$

$$\partial_z T - Bi^b T = \text{constant.}$$

and at the top undeformable free surface:

$$\omega = 0$$

$$-Ma\partial_x T = \partial_z u$$

$$-Ma\partial_y T = \partial_z v$$

$$\partial_z T + Bi^t T = \text{constant.}$$

To study the transition between the motionless conduction state and the convective state, and the evolution of the structures that appear in this convective state, we use a multiple scale perturbation analysis in the vicinity of the onset of convection. We define a small parameter in order to separate the fast variables that describe the instability and the slow ones that are useful to describe the pattern dynamics. Further technical details are given elsewhere [31]. The temperature dependence for a hexagonal pattern reads as:

$$T = T(z)[A_1(X, Y, \tau)\exp(i\mathbf{k}^{(1)}\cdot\mathbf{r}) + A_2\exp(i\mathbf{k}^{(2)}\cdot\mathbf{r}) + A_3\exp(i\mathbf{k}^{(3)}\cdot\mathbf{r}) + c.c.] \tag{4}$$

where $\mathbf{k}^{(i)}$ denotes three linearly critical wave vectors oriented at 120 degrees in the horizontal plane. The amplitude equations in the horizontal plane are (e.g. for A_1):

$$\begin{aligned}\alpha_t\partial_t A_1 = {} & \alpha_l\varepsilon A_1 + \alpha_d(\mathbf{k}^{(1)}\cdot\nabla_x)^2 A_1 + \alpha_q A_2^* A_3^* \\ & - g_d|A_1|^2 A_1 - g_{nd}(|A_2|^2 + |A_3|^2)A_1 \\ & + i\beta_1[A_3^*(\mathbf{k}^{(2)}\cdot\nabla_x)A_2^* + A_2^*(\mathbf{k}^{(3)}\cdot\nabla_x)A_3^*] \\ & + i\beta_2[A_2^*(\mathbf{k}^{(2)}\cdot\nabla_x)A_3^* + A_3^*(\mathbf{k}^{(3)}\cdot\nabla_x)A_2^*],\end{aligned} \tag{5}$$

where

$$\alpha_l = 263.68$$

$$\alpha_t = 43.96 + 11.21\,\mathrm{Pr}^{-1}$$

$$\alpha_q = 97.72 - 22.2\,\mathrm{Pr}^{-1}$$

$$g_d = 425.1 + 132.6\,\mathrm{Pr}^{-1} + 20.82\,\mathrm{Pr}^{-2}$$

$$g_{nd} = 579.8 + 289.3\,\mathrm{Pr}^{-1} + 3.48\,\mathrm{Pr}^{-2}$$

$$\alpha_d = 18.56$$

$$\beta_1 = -30.65 - 7.96\,\mathrm{Pr}^{-1}$$

$$\beta_2 = -124.2 - 0.51\,\mathrm{Pr}^{-1}$$

$$\varepsilon = (Ma - Ma_c)/Ma_c.$$

Similar equations exist for A_2 and A_3 (with circular permutation of the indices). The amplitude equations describe the pattern dynamics of the hexagonal structure for a weakly supercritical region past the instability threshold. The numerical values of the coefficients correspond to the specific case of a poor conducting open, upper surface, $Bi^t = 0$ and good conducting rigid, lower plate, $Bi^b \to \infty$ which are typical of Bénard and Koschmieder experiments. Other thermal conditions at the top (superscript "t") and bottom (superscript "b") merely change the numerical values of the coefficients.

The equations (5) are generalized Ginzburg-Landau equations with genuinely new advective terms when $\beta_i \neq 0$. For the system of these equations there is no Lyapunov functional, hence for some value of the βs we may never reach steady convection. This possible unsteadiness at large times leading to a seemingly chaotic flow pattern may well be considered as a form of interfacial turbulence in a dissipative flow. For a variational problem, when $\beta_i = 0$ say, the Lyapunov functional allows to write (5) in the form:

$$\alpha_t \partial_t A_j = -\frac{\delta \mathscr{L}}{\delta A_j^*}$$

with

$$\mathscr{L} = \int\int dx\, dy \sum_{j=1}^{3} \left[-\alpha_l \varepsilon |A_j|^2 + \alpha_d |(\mathbf{k}^{(j)} \cdot \nabla_x) A_j|^2 + \frac{g_d}{2} |A_j|^4 \right]$$

$$+ g_{nd} [|A_1|^2 |A_2|^2 + |A_1|^2 |A_3|^2 + |A_2|^2 |A_3|^2] + \alpha_q [A_1 A_2 A_3 + c.c.].$$

The amplitude equations for two modes A_1 and A_2 forming an arbitrary angle θ can also be derived using the same procedure as for an hexagonal pattern. Further details about symmetries and related technical matters can be found in Refs. [31–32]. The temperature dependence in this case is:

$$T = T(z) [A_1 \exp(i\mathbf{k}^{(1)} \cdot \mathbf{r}) + A_2 \exp(i\mathbf{k}^{(2)} \cdot \mathbf{r}) + c.c.] \tag{6}$$

where $\mathbf{k}^{(1)} \cdot \mathbf{k}^{(2)} = k^2 \cos\theta = k^2 \beta$. For the two-mode equations, the quadratic terms $A_2^* A_3^*$ and the advective terms (with coefficients β_1 and β_2) do not appear.

Applying the solvability condition, we get

$$\alpha_t \partial_t A_1 = \alpha_l \varepsilon A_1 + \alpha_d (\mathbf{k}^{(1)} \cdot \nabla_x)^2 A_1 - g_d |A_1|^2 A_1 - g_\theta (|A_2|^2) A_1$$

and a similar equation for A_2 (interchanging the indices 1 and 2). The numerical values of the coefficients are the same as for the hexagons except for g_θ, the cubic interaction term. This term has to be computed for each value of the angle θ (as the second order solution depends on θ).

The relative stability of steady platforms (hexagons, squares and rolls) has been studied by varying the parameters of the system. The results summarized in phase

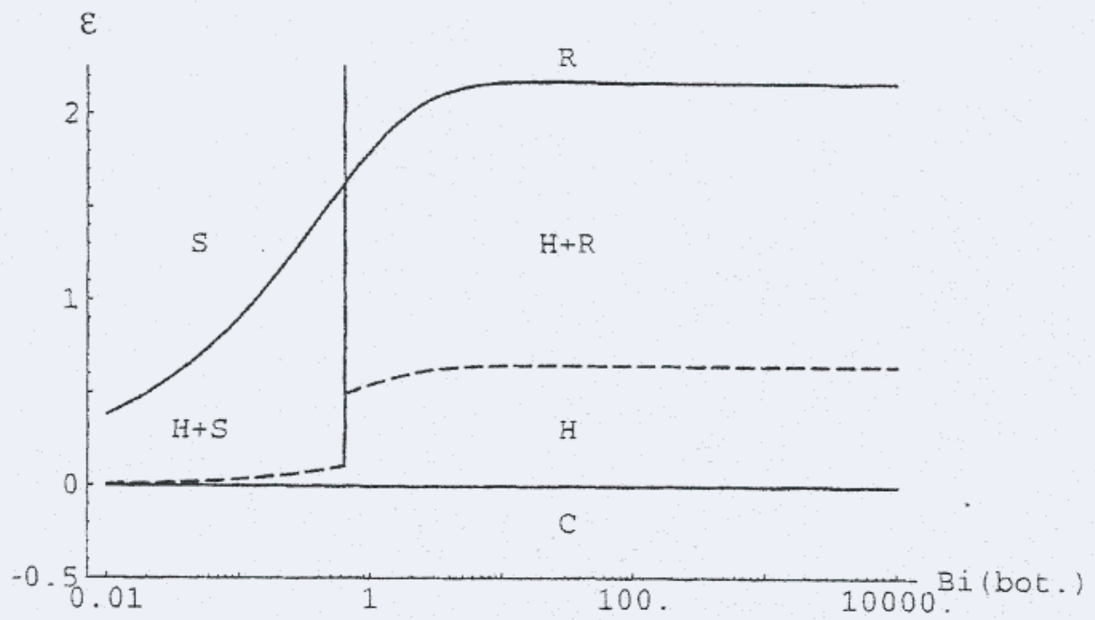

Fig. 2: Local stability of different patterns for $Bi^t = 0$. $Pr \to \infty$. The dashed lines correspond to hysteretic transitions [31].

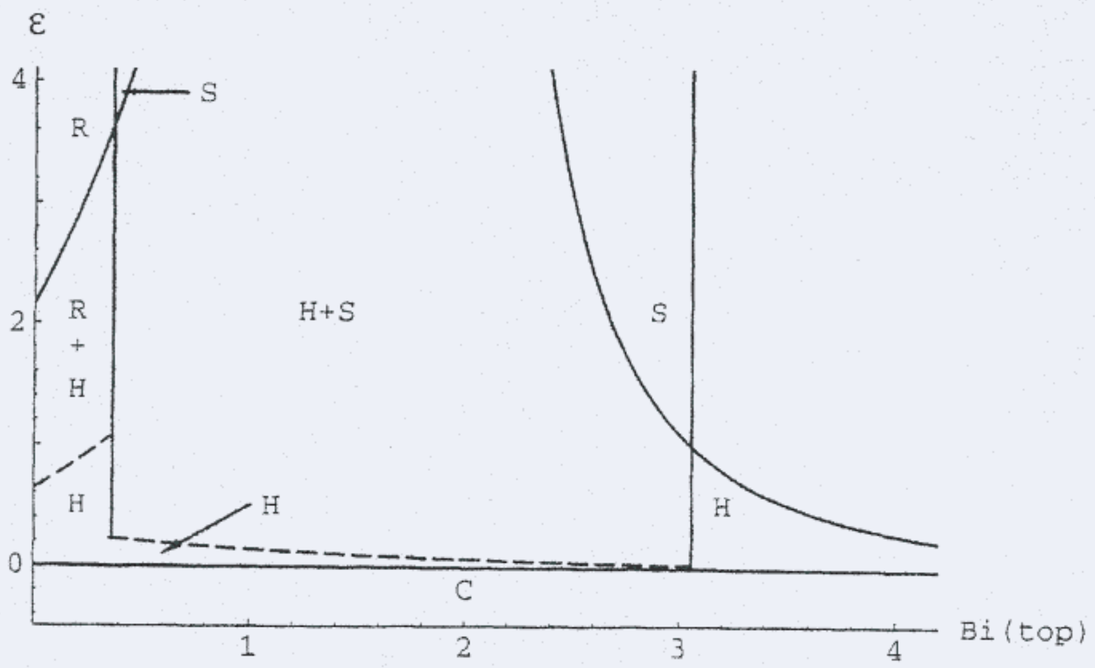

Fig. 3: Local stability of different patterns for $Bi^b \to \infty$. $Pr \to \infty$. The dashed lines correspond to hysteretic transitions [31].

diagrams (Figs. 2 and 3), in the case of large Prandtl number, show the possibility of coexistence of stable patterns. Thus upon increasing the value ε, we cross two coexistence domains. First we cross the coexistence between the motionless state and hexagons, and later on the coexistence between two different types of pattern.

4. Numerical results

Earlier work on the integration of the Boussinesq equations for the Bénard-Marangoni problem dealt with the emergence of the hexagonal pattern above threshold [17, 45]. Other studies of the emergence of patterns, especially in Rayleigh-Bénard convection have used approximate models, e.g. the Swift-Hohenberg [46] variational model and Knobloch's non-variational model [47] which is also valid for Bénard-Marangoni convection. Interesting to be noted is that in the buoyancy-driven, Rayleigh-Bénard problem, the latest available derivation of amplitude equations for rolls due to Zippelius and Siggia (1983) [48] included a non-relaxational term added ad hoc to the Newell-Whitehead equation [39] to account for finite values of the Prandtl number.

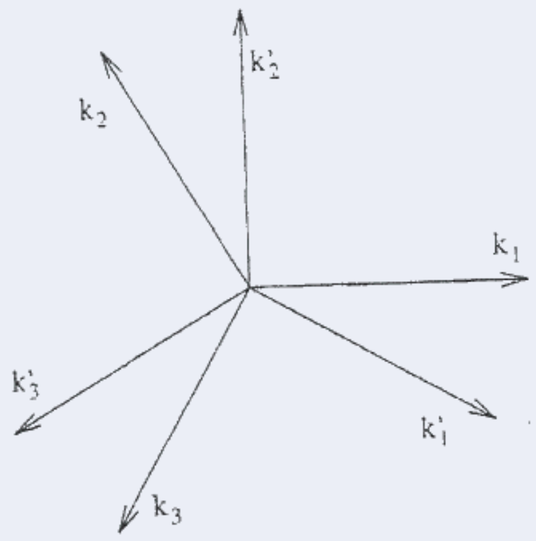

Fig. 4: Two triads of resonant wavevectors $\mathbf{k}_c$ and $\mathbf{k}'_c$ in the horizontal plane (x, y) forming an angle of 30 degrees, one with one other.

Then due to this non-variational term, even at lowest order, there could be an internal vorticity generation that destabilizes the pattern. In our surface tension gradient-driven (Bénard-Marangoni) problem the amplitude equations have non-variational terms even at $Pr \to \infty$ and we shall discuss further below the relevance of this finding to experiments [6, 26, 49, 50]. The latter treated the problem of non-Boussinesq fluids with temperature-dependent viscosity.

Let us see the results of numerical integration of the amplitude equations (5) in a square geometry, starting from random initial conditions. We integrate two families of amplitude equations (6 complex amplitudes) (see Fig. 4) to allow for the possibility to obtain hexagons, squares and rolls. We have used a finite difference method with a semi-implicit scheme (second order in space and first order in time). The details of the method can be found in Christov *et al.* [51]. We followed the time evolution of the patterns by monitoring a norm that measures the distance between two successive convective states of the system, hence a norm sensitive to both amplitude and phase variations. The norm is:

$$L_1 = \frac{1}{\Delta t} \frac{\Sigma_{i,j,k} |A_k^{n+1}(i,j) - A_k^n(i,j)|}{\Sigma_{i,j,k} |A_k^{n+1}(i,j)|}, \tag{7}$$

where the sums run over the i and j points of the spatial grid, and n is the time counter. A constant decaying value of L_1 ensures the settling of the system in a steady state, that may eventually be not the case due to the non-variational terms in Eqs.(5).

Figure 5 displays the time evolution of the reconstructed horizontal temperature field from the amplitudes

$$T(x,y,t) \propto \sum_i A_i \exp(\mathbf{k}_i \cdot \mathbf{r}) + c.c.$$

The simulation was performed in a square geometry with 8 critical wavelengths as side length, and $\varepsilon = 0.063$, $\beta_i = 0$ (variational case). The norm L_1 versus time shows that we asymptotically tend towards a stationary state. Another numerical simulation with the same parameters except that $\beta_i \neq 0$ have been performed and we also observe a monotonic convergence until a final steady state is reached.

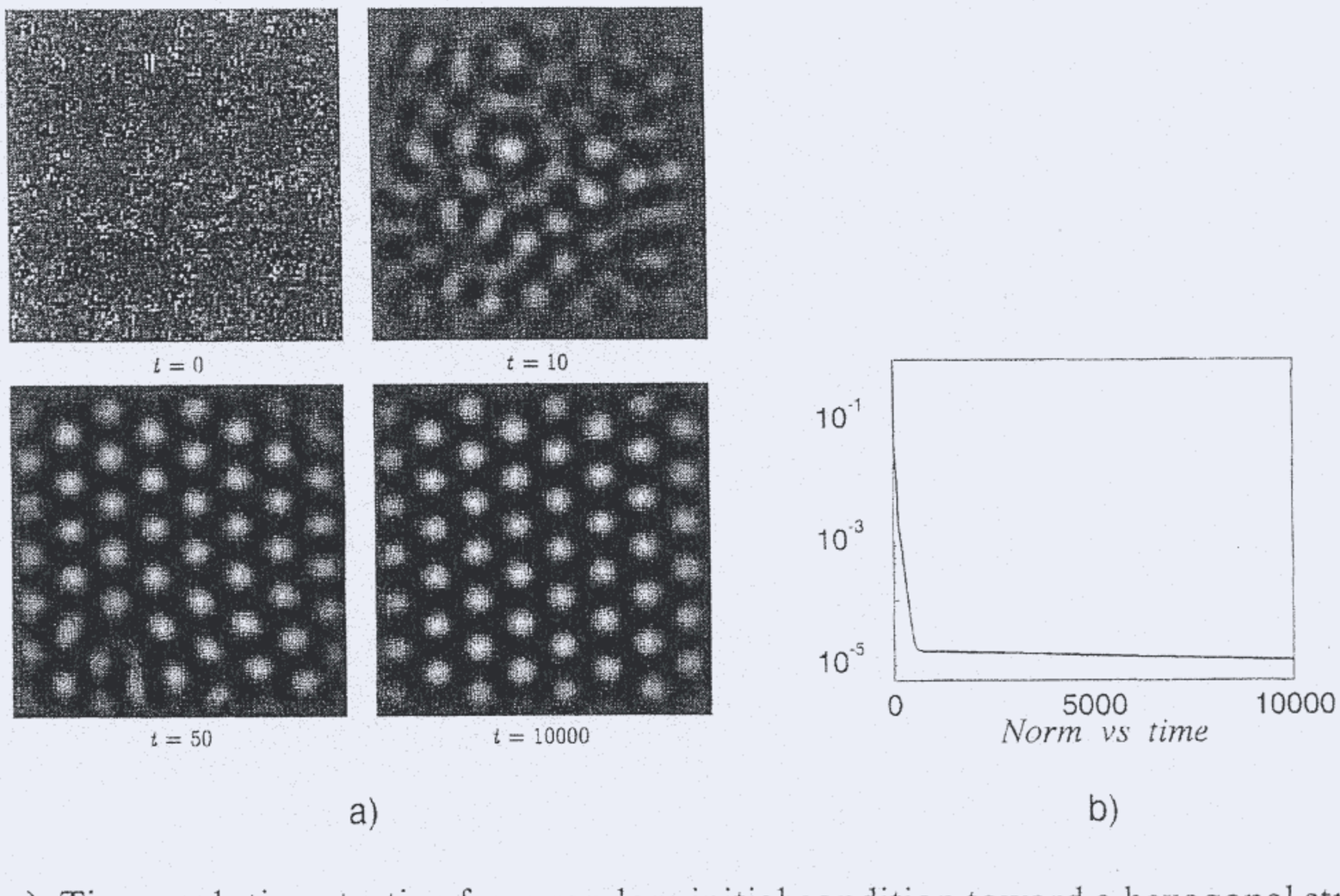

Fig. 5: a) Time evolution starting from random initial condition toward a hexagonal structure, with $\varepsilon = 0.063$, $\beta_i = 0$. **b)** How the initial condition relaxes toward the final state is illustrated by the evolution of the norm L_1. The values of the coefficients entering in the amplitude equations are those given in Eqs. 5 with $Pr \to \infty$, [31].

Figure 6 corresponds to the computation for $\varepsilon = 0.63$ and $\beta_i \neq 0$. The hexagons are no longer stable and a roll structure appears. However, the latter does not settle as pulsating hexagons periodically destabilize the roll pattern at all times. In the experiments, the value $\varepsilon = 0.63$ is too small to allow the observation of such pulsating action of hexagons on rolls. However, experiments by both Koschmieder and Cerisier have shown hexagons albeit with many defects. The apparent disagreement of the numerical simulations and the experiments may come from the fact that more than 6 complex amplitudes are needed to describe the system even for such low value of the supercriticality. Actually, in practical terms, the validity of the description of the convection by amplitude equations appears to be much more limited than expected. The introduction of non-variational terms into the amplitude equations drastically reduces the limit of validity of the description of the convection through amplitude equations. Indeed, a computation conducted for the same values of the parameters but with $\beta_i = 0$ shows that the system still monotonically relaxes toward a final, steady hexagonal structure. The possible coexistence of hexagons and rolls in a layer of fluid with variable thickness has been observed in the experiment of Schatz *et al.* [26].

In Figure 7 appears the time evolution towards the roll structure that settles for large enough supercriticality. In both cases, $\beta_i = 0$ and $\beta_i \neq 0$, the system monotonically evolves towards a final, steady state of rolls. Worth mentioning is that the rate of convergence to a steady state is faster in the non-variational case than in the variational case. A variational dynamics has a higher structural rigidity of its phase space relative to the non-variational case and, consequently, does not allow a fast relaxation.

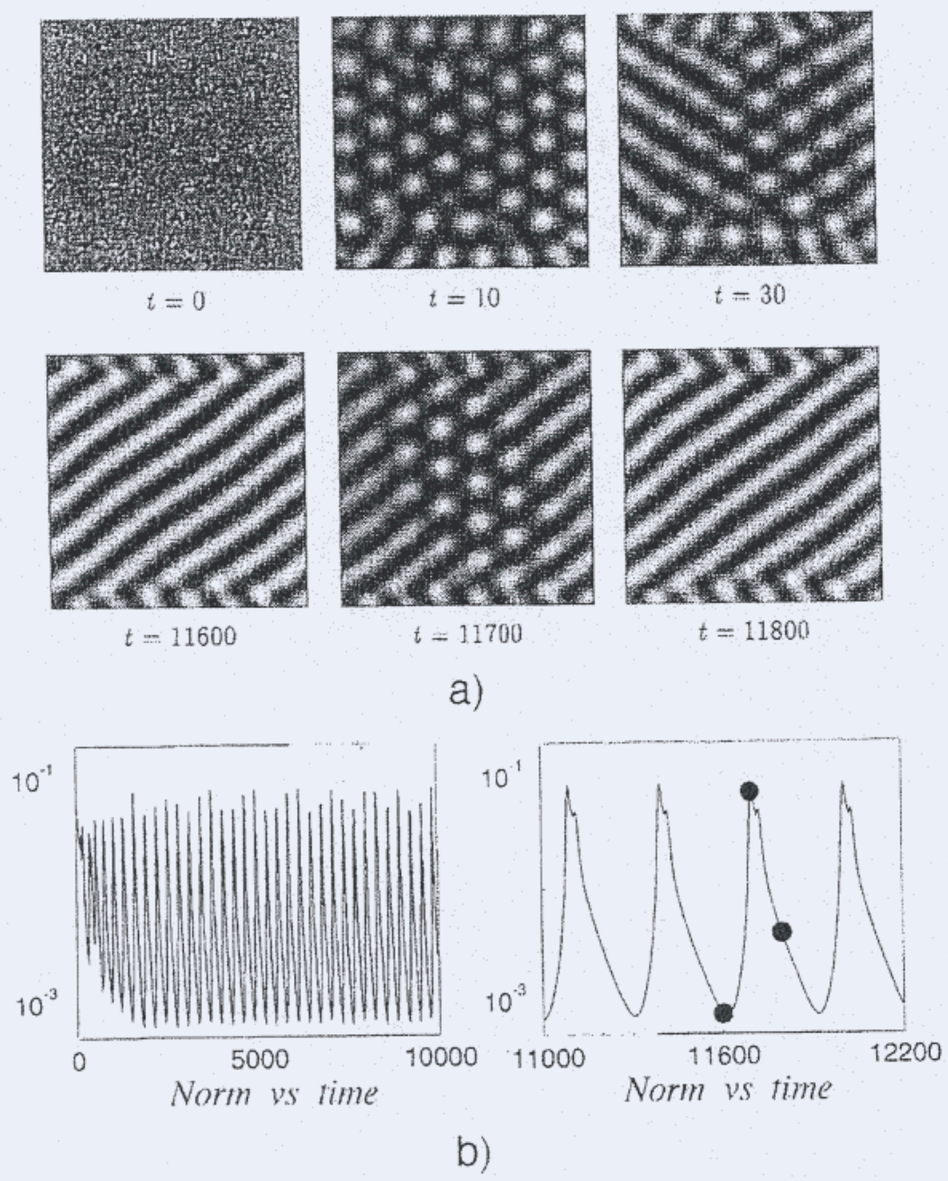

Fig. 6: a) Pulsating evolution (rolls-hexagons) with $\varepsilon = 0.63$, starting from a random initial condition. **b)** The norm L_1 exhibits the periodicity with time. The values of the coefficients entering in the amplitude equations are those given in Eqs. 5 with $Pr \to \infty$, [31].

Figure 8 illustrates the formation of a square pattern, some time ago observed in experiment by White [50] and also found recently as the result of a secondary instability of the hexagons [30]. A finite Biot number at the top interface appears to be responsible for the appearance of such square pattern. Koschmieder and Prahl [52] also found squares in small (aspect-ratio) boxes, a finding theoretically supported by the work of Dauby and Lebon [36].

5. Eckhaus instability

The Eckhaus instability corresponds to the modulation of the wavenumber of the pattern (see, e.g. [4, 53]). Caroli *et al.* [54] and Sushchik and Tsimring [55] have studied the Eckhaus instability of a hexagonal pattern using amplitude equations but without nonlinear spatial terms. In a previous article [31], we generalized these studies to the non variational case. Physically, the Eckhaus instability is responsible for the creation and anihilation of convective cells.

Koschmieder [6], has reported on several experiments dealing with the size of the wavenumber for supercritical values in Bénard convection. Bénard [3] himself reported that the dimension of the cells in his experiments had a minimum at a temperature slightly above the temperature at which the pattern disappeared. Koschmieder [56] and Koschmieder and Switzer [57] in their experiments agree with Bénard's findings.

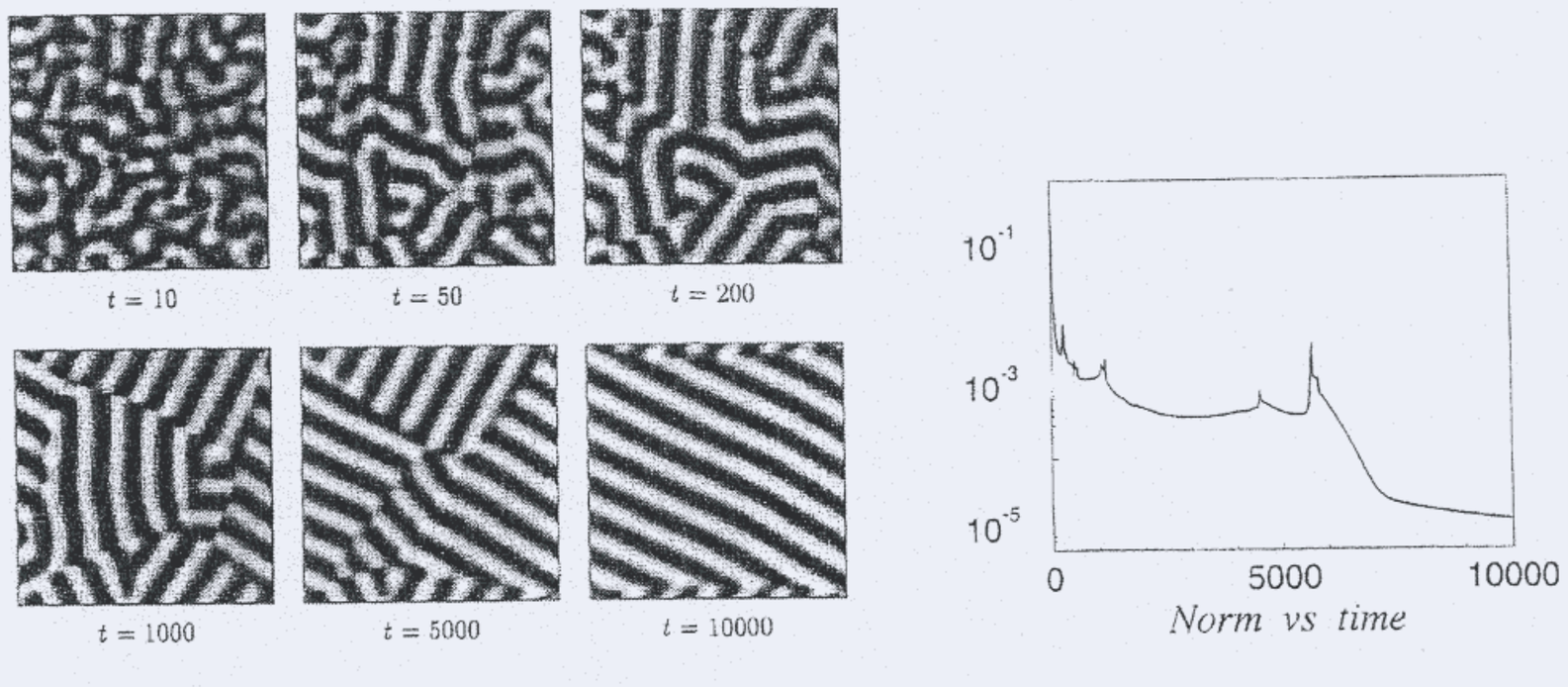

Fig. 7: a) Time evolution starting from a random initial condition toward a roll structure with $\varepsilon = 2.52$, $\beta_i = 0$. **b)** How the initial condition relaxes toward the final state is illustrated by the evolution of the norm L_1. The values of the coefficients entering in the amplitude equations are those given in Eqs. 5 with $Pr \to \infty$, [31].

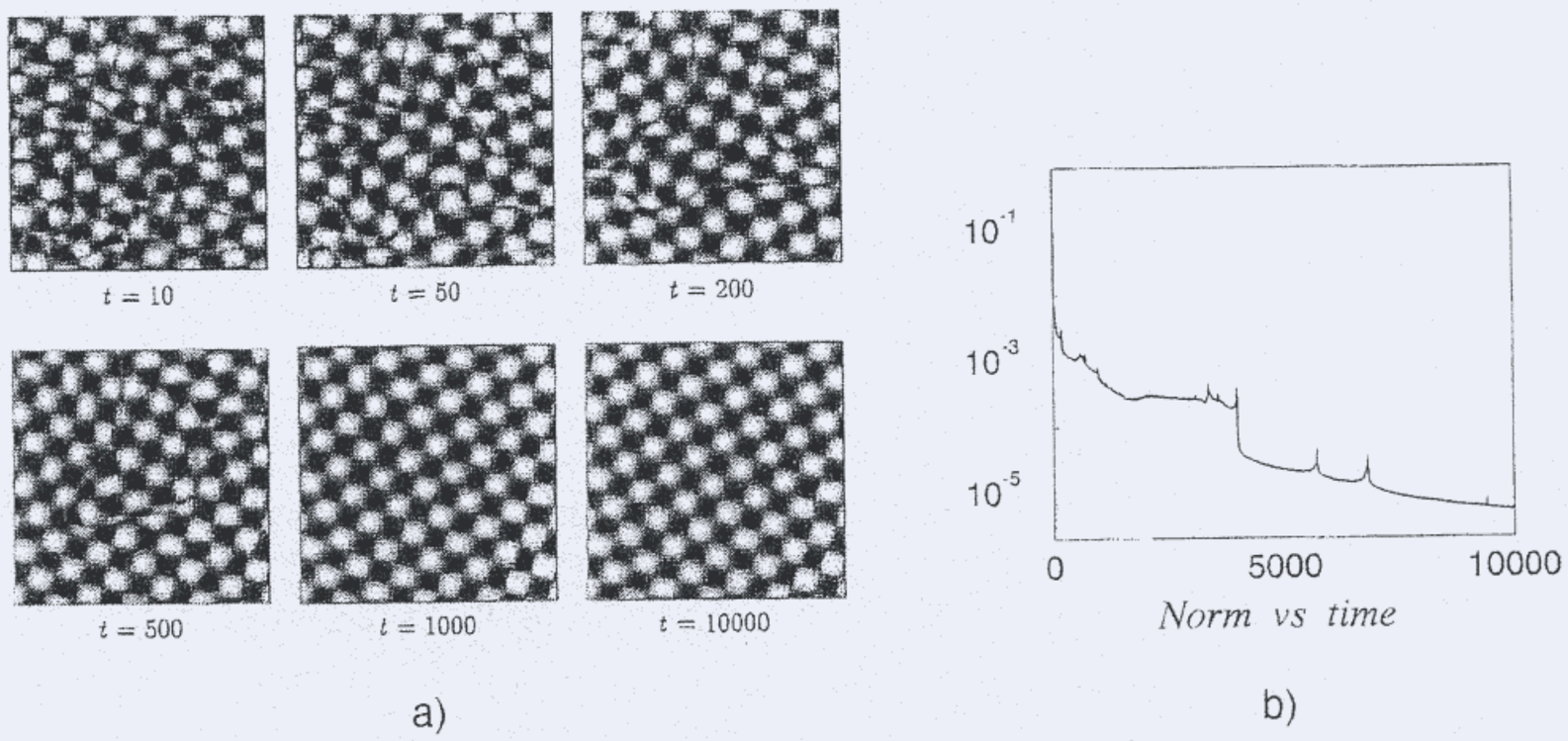

Fig. 8: a) Time evolution starting from a random initial condition toward a square pattern with $\varepsilon = 2.$, $\beta_i = 0.$ starting from random initial condition. **b)** How the initial condition relaxes toward the final state is illustrated by the evolution of the norm L_1. The values of the coefficients entering in the amplitude equations correspond to $Bi^t = 2$, $Bi^b \to \infty$ and $Pr \to \infty$, [31].

Dauzère [58] and Cerisier *et al.* [49] found the opposite result. They observed an increase in the cell size with increasing Marangoni number. Cerisier *et al.* plotted the slope of the wavelength λ versus $\varepsilon = (Ma - Ma^c)/Ma^c$ and they obtained $d\lambda/d\varepsilon = 0.06$. This result corresponds to the dotted line in Figure 9. The experiment was performed using silicone oil in a layer of about 1.62 mm thickness which favours surface tension effects rather than buoyancy. The value of the critical wavenumber was about 2.12. In Figure 9 we have redrawn their results to fit with the critical wavenumber $k_c = 1.99$. Koschmieder and Switzer [57] obtained a trend that was just opposite: a growth of the number of convective cells upon increasing the supercritical heating. The points in Figure 9 are gathered from their experiment with a 1.2 mm fluid layer thickness. For this experiment

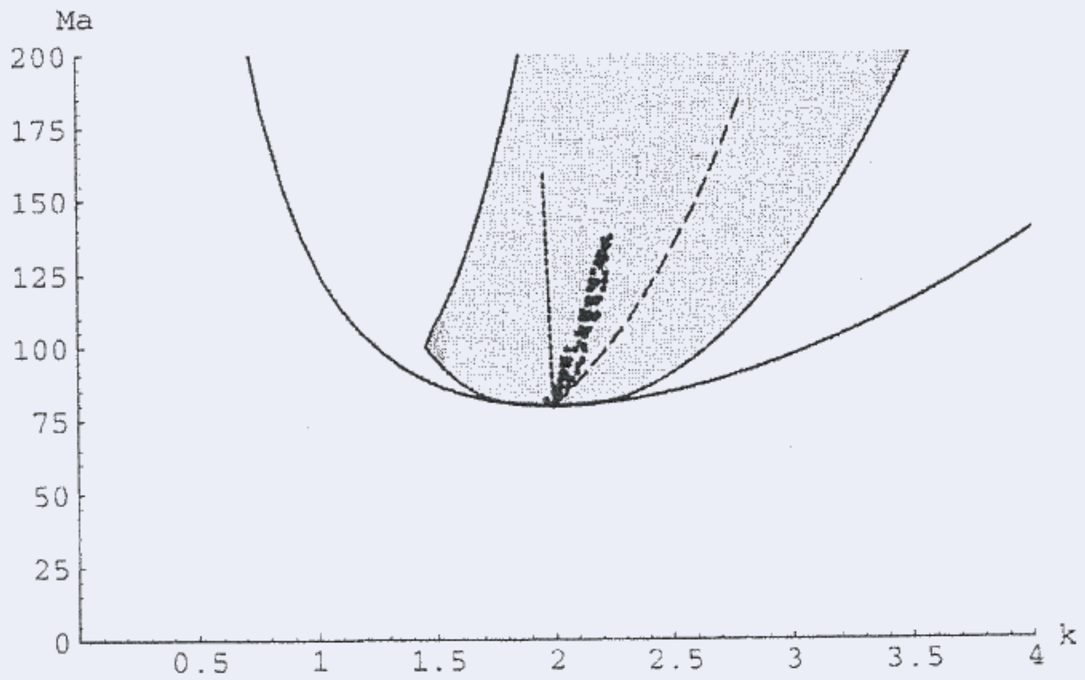

Fig. 9. Eckhaus band in the (k, Ma) plane. The broken line corresponds to the locus of wavenumbers with maximum linear growth rate. The cluster of points corresponds to the data reported by Koschmieder and Switzer [49] while the dotted line corresponds to the experiment by Cerisier *et al.* [43].

they also used silicone oil and the critical wavenumber was about 1.85. In Figure 9, we also shift the origin of their critical point to fit the theoretical value. Figure 9 also displays the corresponding Eckhaus band (for values of $\beta_1 = -0.345, \beta_2 = -1.4, \gamma = 1.36$) which are the theoretical values corresponding to the experiments and the dashed line corresponds to the locus of the theoretical linear maximum growth rate. It clearly appears that both experimental results lay in the Eckhaus band. Koschmieder's results are closer to the theoretical curve corresponding to the maximum growth rate. The conflicting trends appearing in the two experiments can be traced back to the different protocoles followed by these two experimenters. Koschmieder increased the temperature quite smoothly, hence a quasi-steady experiment. At variance with Koschmieder, Cerisier increased the temperature rather suddenly with the expected consequence that more non-linear processes are involved in the dynamics of wavenumber selection, or too long relaxation times beyond their observational time, hence a different result.

6. Defects and complex convection structures

The presence of inhomogeneities or defects in patterns found far from thermodynamic equilibrium is nowadays a well established experimental fact [59]. However, the defects that appear in hexagonal patterns have not yet fully been studied. The dynamics of such defects is quite complicated and the analytical tools to deal with the problem are not simple. In the system of three complex amplitude equations we can write for an hepta-penta defect:

$$A_1 = A_0 \tanh(\alpha\sqrt{(X_1 - X_1^0) + (Y_1 - Y_1^0)^2}) \quad \phi_1 = \arctan\frac{Y_1 - Y_1^0}{X_1 - X_1^0} + \phi_0$$

$$A_2 = A_0 \tanh(\alpha\sqrt{(X_1 - X_2^0) + (Y_2 - Y_2^0)^2}) \quad \phi_1 = \arctan\frac{Y_2 - Y_2^0}{X_2 - X_2^0} \tag{8}$$

$$A_3 = A_0 \quad \phi_3 = 0.$$

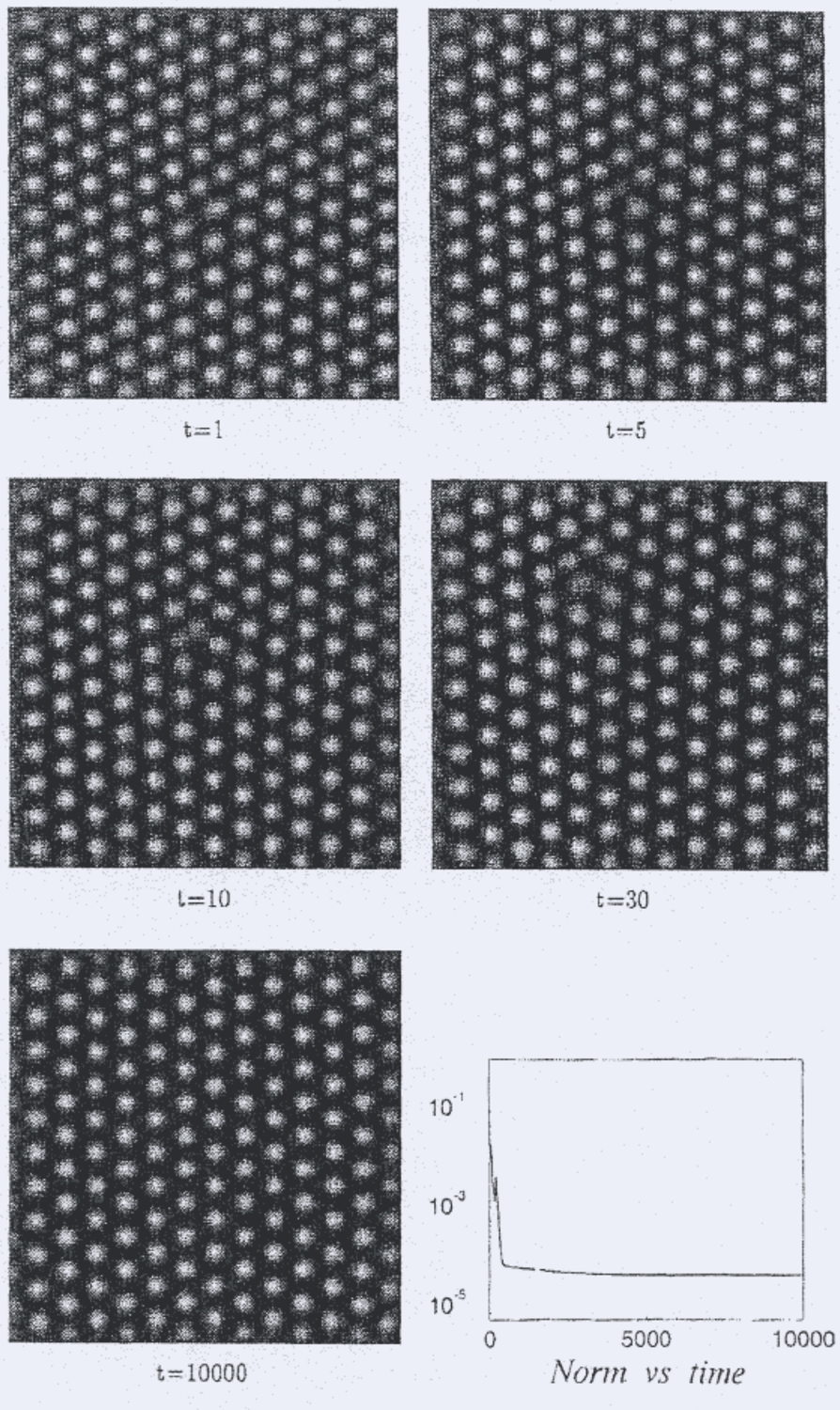

Fig. 10. Time evolution of an hepta-penta defect with $Ma = 85$. The norm L_1 relaxes toward a stationary state. The values of the coefficients entering in the amplitude equations are those given in Eqs. 5 with $Pr \to 0$, [31].

The hepta-penta defect comes from the annihilation of two "vortex" defects of opposite topological charge. The hepta-penta defect after its creation tends to move through the system until it reaches a boundary where it disappears. Tsimring [60] has studied the velocity of such a penta-hepta defect and the mobility tensor related to the defect. His study used a variational amplitude equation. Preliminary numerical exploration (Fig. 10) already indicates that the relaxation of a hepta-penta defect is much easier in the non-variational case as the structural rigidity of the system is diminished in the latter case.

Recent experiments on buoyancy-driven (Rayleigh-Bénard) convection by Assenheimer and Steinberg [61–63] have shown complex convection structures that were earlier observed also by Orell and Westwater [64] and Linde [65] in the mass transfer Bénard-Marangoni problem. The convective structures that have been observed by Assenheimer and Steinberg are spiral, target patterns, and the transition from hexagons to a labyrinthine structure. Assenheimer and Steinberg's experiment deals with a fluid (SF_6) close to its critical thermodynamic point, in a system with quite large aspect

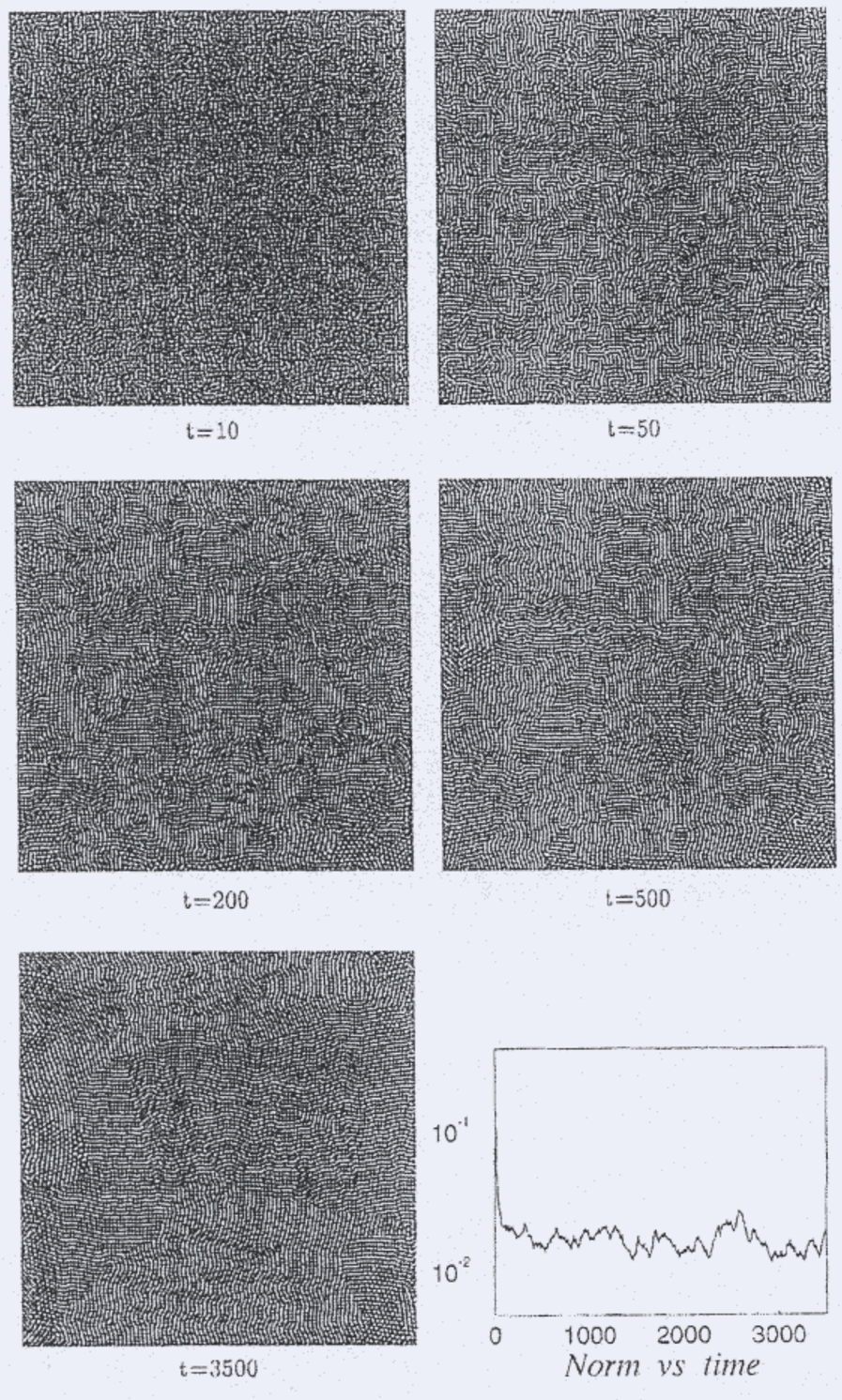

Fig. 11. Time evolution, starting from random initial condition, toward a labyrinthine structure with $Ma = 1.5\, Ma_c$. The norm L_1 does not relax toward a stationary state. The values of the coefficients entering in the amplitude equations are those given in Eqs. 5 with $Pr \to \infty$, [31].

ratio, and however, a not too long time scale. Let us see how these complex structures are predicted from our amplitude equations but for Bénard-Marangoni convection. Integrating the amplitude equations (5) for parameters value close to the "suspected" transition from hexagons to the labyrinthine structure, we found indeed an astonishingly labyrinthine structure. Figure 11 shows the evolution of the structure for a large aspect ratio.

7. Conclusions

Although Bénard convection, since the pioneer has received due attention by careful experimenters like Koschmieder and others, and significant understanding has been achieved, yet surface tension gradient-driven (Bénard-Marangoni) convection flows still deserve further study. Indeed, as a paradigmatic form of a spontaneous self-organizing system, the doctrine about the original Bénard problem has not reached the degree of sophistication, in theory and experimentation, attained in buoyancy-driven (Rayleigh-Bénard)) convection. Needless to say, one reason is the relative higher difficulty of conducting a clean, clear-cut controlled experiment when surface tension

gradients are involved. It is only quite recently that appropriate techniques, to carefully handle surface tension and surface tension gradient-driven phenomena, have become available. As surface tension gradient-driven flows are of utmost importance for heat and mass transfer across interfaces, crystal growth, and other engineering processes this adds interest to further study the problem.

Here we have described some of the major findings, old and recent, about Bénard convection. Theoretical, analytical and numerical as well as experimental results, clearly illustrate the richness of the phenomena predicted and observed. Among the results to be highlighted are the theoretical prediction that, in Bénard convection, attaining a steady state with time independent constraints may, however, not always be the case. The origin of this asymptotic unsteadiness, hence possible space and time chaos or interfacial turbulence even at low Marangoni number, can be traced back to the lack of a variational principle (a Lyapunov function) governing the evolution of the system even in a vicinity of the instability threshold. Although the (full, nonlinear) Navier-Stokes equations (and the heat equation) with corresponding boundary conditions cannot be derived from a potential yet we know that in many cases, when the system is studied in the neighborhood of an instability point, suitable variational equations describe its evolution. This is, generally, not the case for Bénard-Marangoni convection. Another salient feature of Bénard convection flows is that for large containers not only standard convection patterns, like hexagons, rolls or squares, regular or with defects, may appear. Our prediction is that labyrinthine, complex flow patterns are possible and have actually been observed albeit in not sufficiently well controlled experiments. Whether these complex patterns, presumably also precursors of interfacial turbulence are actually realizable in carefully controlled experiments is not unexpected in view of the non-variational character of the evolution equations describing Bénard convection flows. Moreover, labyrinthine flows have already been observed in some cases of buoyancy-driven (Rayleigh-Bénard) convection. Thus, in view of the universality of the theoretical and experimental results here discussed, further theoretical and experimental works are foreseing in the near future about Bénard convection flows, both at low and high Marangoni numbers.

Acknowledgements

The authors have benefited from fruitful discussions with A. A. Nepomnyashchy, A. Golovin, C. I. Christov and J. Pontes. This research has been supported by the European Union under Grants ERBCHBICT 941046 (J. B., level 20 fellowship), 106 and 107 (Networks), by DGICYT (Spain) Grant PB 93–81, by Fundación "Ramón Areces" and by Foundación BBV (Programa Catedra Cambridge University).

References

[1] Rowlinson, J. S., Widom, B., Molecular theory of capilarity, Clarendon Press, Oxford, 1982.
[2] Levich, V. G., Physicochemical Hydrodynamics, Prentice-Hall, Englewood Cliffs, NJ, 1962.

[3] Bénard, H., Les tourbillons cellulaires dans une nappe liquide, Rev. Gén. Sciences Pure Appl., 11 (1990), 1261–1271.
[4] Normand, C., Pomeau, Y., Velarde, M. G., Convective instability: A physicist's approach, Rev. Mod. Phys., 49 (1977), 581–624.
[5] Velarde, M. G., Normand, C., Convection, Sci. Am., 243 (1980), 92–108.
[6] Koschmieder, E. L., Bénard Cells and Taylor Vortices, Cambridge Univ. Press, Cambridge, UK, 1993.
[7] Thomson, J., On certain curious motions observale at the surfaces of wine and other alcoholic liquors, Philos. Mag., 10 (1855), 330.
[8] Thomson, J., On a changing tessellated structure in certain fluid, Proc. Roy. Phil. Soc. (Glasgow), 13 (1882), 464.
[9] Weber, E. H., Mikroskopische Beobachtungen sehr gesetzmässiger Bewegungen, welche die Bildung von Niederschlägen harziger Körper aus Weingeist begleiten. Ann. Phys. (Poggendorf), 94 (1855), 447.
[10] Velarde, M. G., Hydrodynamic Instabilities, in: Fluid Dynamics, Eds. R. Balian and J. L. Peube, pages 469–527, Gordon and Breach, New York, 1976.
[11] Block, M. J., Surface tension as the cause of Bénard cells and surface deformation in a liquid film, Nature, 178 (1956), 650–651.
[12] Lord Rayleigh, On the dynamics of revolving fluids, Proc. R. Soc. London Ser. A, 93 (1916), 148.
[13] Velarde, M. G., Castillo, J. L., Transport and reactive phenomena leading to interfacial instability, in: Convective transport and instability phenomena, Eds. J. Zierep and H. Oertel, pages 235–264, Braun-Verlag, Karlsruhe, 1982.
[14] Pearson, J. R. A., On convection cells induced by surface tension, J. Fluid Mech., 4 (1958), 489–500.
[15] Davis, S. H., Thermocapillary instabilities, Ann. Rev. Fluid Mech., 19 (1987), 403–435.
[16] Cross, M. C., Hohenberg, P. C., Pattern formation outside of equilibrium, Rev. Mod. Phys., 65 (1993), 851–1112.
[17] Thess, A., Orzag, S. A, Surface-tension-driven Bénard convection at infinite Prandtl number, J. Fluid Mech., 283 (1995), 201–230.
[18] Scanlon, J. W., Segel, L. A., Finite amplitude cellular convection induced by surface tension, J. Fluid Mech., 30 (1967), 149–162.
[19] Levchenko, E. B., Chernyakov, A. L., Instability of surface waves in a nonuniformly heated liquid, Sov. Phys. JET P, 54 (1981), 102.
[20] García-Ybarra, Castillo, P. L., Velarde, M. G., Bénard-Marangoni convection with a deformable interface and poorly conducting boundaries, Phys. Fluids, 30 (1987), 2655–2661.
[21] García-Ybarra, J. L., Castillo, P. L., Velarde, M. G., A non-linear evolution equation for Bénard-Marangoni convection with deformable boundary, Phys. Lett. A, 122 (1987), 107–110.
[22] Chu, X. L., Velarde, M. G., Transverse and longitudinal waves induced and sustained by surfactant gradients at liquid-liquid interfaces, J. Coll. Int. Sci., 131 (1989), 471–484.
[23] Cloot, A., Lebon, G., A non-linear stability analysis of the Bénard-Marangoni problem, J. Fluid Mech., 145 (1984), 447–469.
[24] Bragard, J., Lebon, G., Non-linear Marangoni convection in a layer of finite depth Europhys. Lett., 21 (1993), 831–836.
[25] Cerisier, P., Jamond, C., Pantaloni, J., Pérez-Garcia, C., Stability of roll and hexagonal patterns in bénard-marangoni convection, Phys. Fluids, 30 (1987), 954–959.
[26] Schatz, M. F., VanHook, S. J., McCormick, W. D., Swift, J. B., Swinney, H. L., Onset of surface-tension-driven Bénard convection, Phys. Rev. Lett., 75 (1995), 1938–1947.
[27] Davis, S. H., Buoyancy-surface tension instability by the method of energy, J. Fluid. Mech., 39 (1969), 347–359.
[28] Davis, S. H., Homsy, G. M., Energy stability theory for free-surface problems: buoyancy-thermocapillary layers, J. Fluid. Mech., 98 (1980), 527.

[29] Castillo, J. L., Velarde, M. G., Buoyancy-thermocapillary instability: the role of interfacial deformation in one- and two-component fluid layers heated from below or above, J. Fluid. Mech., 125 (1982), 463.
[30] Nitschke, K., Thess, A., Secondary instability in surface tension driven Bénard convection, Phys. Rev. E, 52 (1995), 5772–5775.
[31] Bragard, J., Velarde, M. G., Bénard-Marangoni Convection: Planforms and related theoretical predictions, J. Fluid Mech., in print (1996).
[32] Gunaratne, G. H., Complex spatial patterns on planar continua, Phys. Rev. Lett. 10 (1993), 1367–1370.
[33] Golovin, A. A., Nepomnyashchy, Pismen, L. M., Pattern formation in large-scale Marangoni convection with deformable interface, Physica D 81 (1995), 117–147.
[34] Hadji, L., Nonlinear analysis of the coupling between interface deflection and hexagonal patterns in Rayleigh-Bénard-Marangoni convection, Phys. Rev. E 53 (1996), 5982–5992.
[35] Kubstrup, C., Herrero, H., Pérez García, C., Fronts between hexagons and squares in a generalized Swift-Hohenberg equation, Phys. Rev. E 54 (1996), 1560–1569.
[36] Dauby, P. C., Lebon, G., Bénard-Marangoni instability in rigid rectangular containers, J. Fluid Mech. 329 (1996), 25–64.
[37] Landau, E. M., On the problem of turbulence, C. R. Acad. Sci. URSS, 44 (1944), 311.
[38] Stuart, J. T., On the nonlinear mechanics of hydrodynamic stability, J. Fluid Mech., 4 (1958), 1–21.
[39] Newell, A. C, Whitehead, J. A, Finite bandwidth, finite amplitude convection, J. Fluid Mech., 38 (1969), 279–303.
[40] Pérez-Cordon, R., Velarde, M. G., On the (non-linear) foundations of Boussinesq approximation applicable to a thin layer of fluid, J. Phys. (*Paris*), 36 (1975), 591.
[41] Velarde, M. G., Pérez-Cordon, R., On the (non-linear) foundations of Boussinesq approximation aplicable to a thin layer of fluid, (ii) viscous dissipation and large cell gap effects, J. Phys. (*Paris*), 37 (1975), 177–182.
[42] Gray, D. D., Giorgini, A., The validity of the Boussinesq approximation for liquids and gases, Int. J. Heat Mass Transfer 19 (1976), 545–551.
[43] de Boer, P. T. C., Thermally driven motion of strongly heated fluids, Int. J. Heat Mass Transfer 27 (1984), 2239–2251.
[44] de Boer, P. T. C., Thermally driven motion of highly viscous fluids, Int. J. Heat Mass Transfer 29 (1986), 681–688.
[45] Bestehorn, M. Phase instabilities for Bénard-Marangoni convection in fluid layers with large aspect ratio, Phys. Rev. E, 48 (1993), 3622–3634.
[46] Swift, J., Hohenberg, P. C., Hydrodynamic fluctuations at the convective instability, Phys. Rev. A, 15 (1977), 319–328.
[47] Knobloch, E., Pattern selection in long-wavelength convection, Physica D, 41 (1990), 450–479.
[48] Zippelius, A., Siggia, E., Stability of finite-amplitude convection, Phys. Fluids, 26 (1983), 2905–2915.
[49] Cerisier, P., Pérez-Garcia, C., Jamond, C., Pantaloni, J., Wavelength selection in Bénard-Marangoni convection, Phys. Rev. A, 35 (1987), 1949–1952.
[50] White, D. B., The planforms and onset of convection with a temperature-dependent viscosity, J. Fluid Mech., 191 (1988), 247–286.
[51] Christov, C. I., Pontes, J. Velarde, M. G., Splitting methods for free-surface viscous fluids subject to thermal Marangoni effects, Comp. Rend. Bulg. Acad. Sci., 39 (1986), 23–26.
[52] Koschmieder, E. L., Prahl, S., Surface tension driven Bénard convection in small containers, J. Fluid Mech. 215 (1990), 571–593.
[53] Wierschem, A., Cesirier P., Gallet P., Velarde, M. G., Creation and extinction of cells in Bénard convection, J. Non-Equilib. Thermodyn. 21 (1997), No. 2, in print.
[54] Caroli, B., Caroli, C., Roulet, B., On the stability of hexagonal interfacial patterns in directional solidification of binary mixtures, J. Crystal Growth, 68 (1984), 677–690.
[55] Sushchik, M. M., Tsimring, L. S., The Eckhaus instability in hexagonal patterns, Physica D, 74 (1994), 90–106.

[56] Koschmieder, E., The wavelength of supercritical surface tension driven Bénard convection, Eur. J. Mech. B/Fluids, 10 (1991), 233–237.
[57] Koschmieder, E., Switzer, D., The wavenumbers of supercritical surface-tension-driven Bénard convection, J. Fluid Mech., 240 (1992), 533–548.
[58] Dauzère, C., Sur les changements qu'éprouvent les tourbillons cellulaires lorsque la température s'élève, Compt. Rend., 155 (1912), 394–398.
[59] Walgraef, D., Structures Spatiales Loin de l'Equilibre, Masson, Paris, 1988.
[60] Tsimring, L. S., Dynamics of penta-hepta defects in hexagonal patterns, Physica D, 89 (1996), 368–380.
[61] Assenheimer, M., Steinberg, V., Transition between spiral pattern and target pattern states in Rayleigh-Bénard convection, Nature, 367 (1994), 345.
[62] Assenheimer, M., Steinberg, V., Critical phenomena in hydrodynamics, Europhys. News, 27 (1996), 143.
[63] Assenheimer, M., Steinberg, V., Observation of coexisting upflow and downflow hexagons in Boussinesq Rayleigh-Bénard convection, Phys. Rev. Lett., 76 (1996), 756–760.
[64] Orell, A., Westwater, J. W., Spontaneous interfacial cellular convection accompanying mass transfer, A.I.Ch.E. Journal, 8 (1962), 350.
[65] Linde, H., Marangoni instabilities. in: Convective transport and instability phenomena, Eds. J. Zierep and H. Oertel, pages 265–296, Braun-Verlag, Karlsruhe, 1982.

Paper received: 1996-12-03
Paper accepted: 1997-01-23

Dr. J. Bragard
Prof. Dr. Manuel G. Velarde
Instituto Pluridisciplinar
Universidad Complutense
Paseo Juan XXIII, no. 1
E-28040 Madrid
Spain